ACS OMEGA

http://pubs.acs.org/journal/acsodf

Article

Comparison of CH_4 and CO_2 Adsorptions onto Calcite(10.4), Aragonite(011)Ca, and Vaterite(010)CO_3 Surfaces: An MD and DFT Investigation

Ming Zhang,* Jian Li,* Junyu Zhao, Youming Cui, and Xian Luo

Cite This: *ACS Omega* 2020, 5, 11369−11377

Read Online

ACCESS | Metrics & More | Article Recommendations | Supporting Information

ABSTRACT: The interaction between greenhouse gases (such as CH_4 and CO_2) and carbonate rocks has a significant impact on carbon transfer among different geochemical reservoirs. Moreover, CH_4 and CO_2 gases usually associate with oil and natural gas reserves, and their adsorption onto sedimentary rocks may influence the exploitation of fossil fuels. By employing the molecular dynamics (MD) and density functional theory (DFT) methods, the adsorptions of CH_4 and CO_2 onto three different $CaCO_3$ polymorphs (i.e., calcite(10.4), aragonite(011)Ca, and vaterite(010)CO_3) are compared in the present work. The calculated adsorption energies (E_{ad}) are always negative for the three substrates, which indicates that their adsorptions are exothermic processes and spontaneous in thermodynamics. The E_{ad} of CO_2 is much more negative, which suggests that the CO_2 adsorption will form stronger interfacial binding compared with the CH_4 adsorption. The adsorption precedence of CH_4 on the three surfaces is aragonite(011)Ca > vaterite(010)CO_3 > calcite(10.4), while for CO_2, the sequence is vaterite(010)CO_3 > aragonite(011)Ca > calcite(10.4). Combining with the interfacial atomic configuration analysis, the Mulliken atomic charge distribution and overlap bond population are discussed. The results demonstrate that the adsorption of CH_4 is physisorption and that its interfacial interaction mainly comes from the electrostatic effects between H in CH_4 and O in CO_3^{2-}, while the CO_2 adsorption is chemisorption and the interfacial binding effect is mainly contributed by the bonds between O in CO_2 and Ca^{2+} and the electrostatic interaction between C in CO_2 and O in CO_3^{2-}.

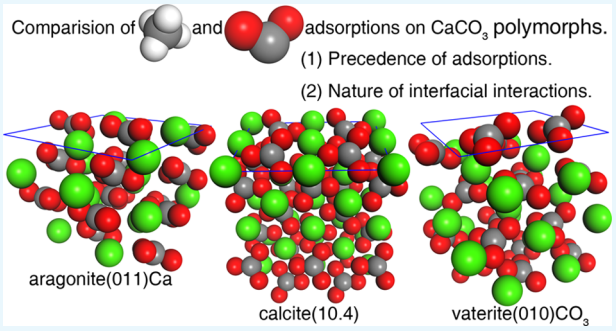

1. INTRODUCTION

Calcium carbonate ($CaCO_3$) extensively exists as sedimentary rocks in the earth's crust.[1,2] The carbonate rocks are expected to influence and regulate the carbon transfer between different geochemical reservoirs.[1,3] It is reported that these minerals might be helpful in converting atmospheric greenhouse gases (such as carbon dioxide and methane) into solid carbonate.[4−6] For instance, $CaCO_3$ can be regarded as the products of CO_2 capture reactions with CaO and can also be decarbonated to CaO;[7] vaterite $CaCO_3$ microspheres can be synthesized and used as a novel CO_2 storage material;[8] and mixed alkali metal salt MgO−$CaCO_3$ sorbents are capable of adsorbing CO_2 at an ultrafast rate, high capacity, and good stability.[9] Thus, carbonate rocks may have an impact on global climate change.

On the other hand, a considerable proportion of the world's oil and natural gas reserve is found associated with carbonate sedimentary rocks, such as limestone, chalk, and dolomite, in which $CaCO_3$ is the main constituent.[10−13] Meanwhile, the injection of carbon dioxide (CO_2) is utilized as an approach to enhance fuels' recovery. So, the interaction between the gas constituents and sedimentary rocks may have an impact on fossil fuels' exploiting efficiency. Until now, the studies on CH_4 and CO_2 adsorptions on carbonate rocks are insufficient. Aiming to make a further clarification of the adsorptions, we have investigated the competitive adsorption of CH_4 and CO_2 onto different polymorphs of $CaCO_3$, which will be helpful in enhancing oil[12] and natural gas[14] recovery rates.

Calcium carbonate ($CaCO_3$) can exist as different polymorphs, in which the three phases of calcite, aragonite, and vaterite are commonly reported, and their thermodynamic stability decreases as per the sequence.[15] Although vaterite is reported to not commonly found in geological conditions, it is an important precursor in several carbonate-forming systems.[15] So, in the present work, all of the three $CaCO_3$ polymorphs are considered.

In recent decades, the methods of DFT calculation and MD simulations have been successfully implemented in the study of

Received: January 24, 2020
Accepted: April 30, 2020
Published: May 11, 2020

https://dx.doi.org/10.1021/acsomega.0c00345
ACS Omega 2020, 5, 11369−11377

molecule adsorption onto carbonate substrates. For instance, for the interaction between water and the calcite(10.4) surface, the dissociated and associated H_2O molecules were compared and the dissociated ones were confirmed as a metastable state.[16] The adsorptions of several organic molecules (hexane, cyclohexane, and benzene) are studied on the surface (10.4) of dolomite $CaMg(CO_3)_2$, and the adsorption energies of these organic molecules are compared with that of the water molecule.[12] Chun et al.[17] characterized the adsorption of benzoate and stearate on the surface of calcite(10.4), and the binding energies of adsorbed molecules were investigated in the presence of water and oil phases. The adsorption energies of a series of small molecules (i.e., water, several alcohols, and acetic acid) were determined and compared on three synthetic $CaCO_3$ polymorphs (calcite, aragonite, and vaterite).[18] Ataman et al.[13,19] investigated the adsorptions of some functional groups on calcite(10.4), including oxygen-, nitrogen-, and sulfur-containing molecules and nonpolar organic molecules.

Narrowly, for the adsorptions of CH_4 and CO_2 onto $CaCO_3$ rocks, several important studies[20−23] can be noted and classified into experimental and theoretical sides:

(1) On the experimental side, the competitive adsorption of CH_4 and CO_2 onto limestone was investigated in the temperature range of 50−150 °C and the higher affinity of CO_2 to the rock was confirmed, which can be ascribed to the strong electrostatic attraction between the CO_2 molecule and limestone.[23] Mixing of 10% CO_2 into CH_4 would enhance the adsorption of methane at 150 °C. Due to the high adsorption affinity of CO_2, the total uptake increased, depending on the CO_2 partial pressure. The adsorption of CO_2 on limestone was confirmed to be four times higher than that of CH_4. The higher natural selectivity of carbonate toward CO_2 was thermodynamically supported by the lower adsorption heat of CO_2.

(2) For theoretical studies of the CH_4[21,22] and CO_2[20−22] adsorptions onto calcite substrates, the methods of MD simulations[20−22] and grand canonical Monte Carlo (GCMC)[21] have been employed. The adsorptions of H_2O, CO_2, CH_4, and N_2 gases on calcite($1\bar{1}0$) are compared, and the preferential order is confirmed as follows: $H_2O > CO_2 > CH_4 > N_2$; CO_2 molecules could form an adsorbed layer on the surface, while no significant feature indicates that CH_4 molecules would be adsorbed on calcite($1\bar{1}0$).[22] Furthermore, the adsorption and diffusion of CH_4 and CO_2 in calcite nanosized pores (width ∼22 Å) were compared, and it was confirmed that CO_2 has much higher adsorption capacity and much less diffusion capacity compared with CH_4.[21] Finally, the adsorption behavior of CO_2 molecules on calcite(10.4) was investigated, which demonstrates that CO_2 molecules would be adsorbed perpendicularly at the sites of Ca ions and the desorption of CO_2 molecules would be positively correlated with temperature.[20]

Based on our literature availability, the hierarchical comparisons of CH_4 and CO_2 adsorptions onto different $CaCO_3$ polymorphs are still insufficient and need further clarification. In the present work, by combining MD and DFT methods, the CH_4 and CO_2 adsorptions onto various $CaCO_3$ polymorphs (i.e., calcite, aragonite, and vaterite) are investigated and compared. The interactions between adsorbents ($CaCO_3$ polymorphs) and adsorbates (gas molecules) are emphasized and compared; therefore, the adsorption systems are specifically studied in vacuum environments. All our DFT calculations are performed on a static molecular system, and the temperature effect is out of discussion in this work (the temperature is fixed at 0 K).

First, bulk unit cells of three $CaCO_3$ polymorphs are established and relaxed with DFT calculations, and the bulk properties, such as lattice parameters and bulk modulus, are calculated. Then, various surfaces are created based on these relaxed unit cells, and the surface energies are examined. After that, the interface systems are established by putting gas molecules on the surfaces, and MD geometry optimizations are conducted for the interface models to achieve rough estimates of atomic configurations. Finally, the rough estimates are continually relaxed with the DFT method to reach their ground states, and based on these final atomic configurations, the remaining properties, such as adsorption energy, electron distribution, and density of states, are determined with the DFT method.

2. RESULTS AND DISCUSSION

2.1. Bulk Calculations. The space groups of calcite and aragonite are experimentally identified as $R\bar{3}c$ (167)[13] and *Pmcn* (62),[24] respectively. However, the space group of vaterite is still in controversy, and based on previous literature works,[25,26] the space group *Pbnm* (62) is adopted in this work. The unit cells of these three polymorphs are depicted in Figure 1.

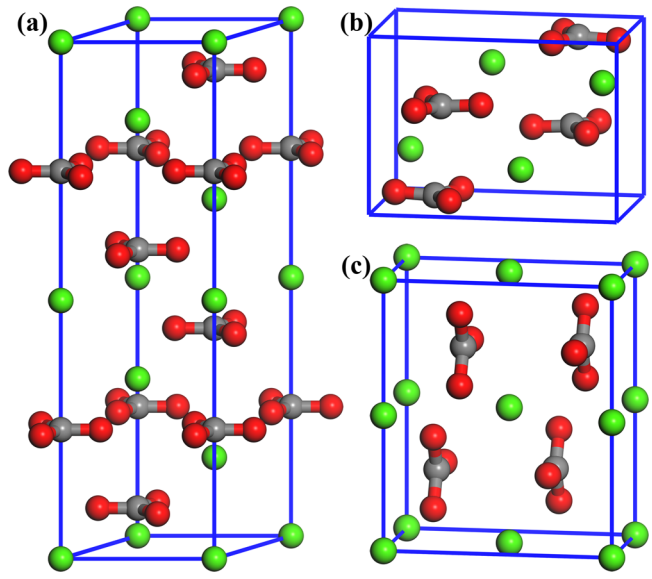

Figure 1. Unit cells of $CaCO_3$ polymorphs: (a) calcite, (b) aragonite, and (c) vaterite. Different color spheres denote Ca (green), O (red), C (dark gray), and H (white) atoms.

The calculated lattice constants (*a*, *b*, and *c*) and bulk moduli (*B*) of bulk calcite, aragonite, and vaterite are listed in Table 1. Our results are in good accordance with the previous experimental and theoretical data. Especially for the lattice constants, they agree well with the experimental data for bulk calcite, aragonite, and vaterite.

2.2. Surface and Interface Models. Surface stability can be characterized by surface energy (γ_s) values; the surface with smaller γ_s is thermodynamically more stable. The surface

https://dx.doi.org/10.1021/acsomega.0c00345
ACS Omega 2020, 5, 11369−11377

Table 1. Lattice Constants (a, b, and c) and Bulk Moduli (B) of Bulk Calcite, Aragonite, and Vaterite

phases	space group	Pearson symbol	Strukturbericht designation	data sources	lattice constants (Å) a	b	c	B (GPa)
calcite	$R\bar{3}c$ (167)	$hR10$	$G0_1$	present work	5.0527	5.0527	17.2510	71.8
				previous calculation	4.797	4.797	17.482[27]	69.6[28]
				previous calculation	5.06	5.06	17.25[13]	75.6[29]
				previous calculation	4.933	4.933	17.242[30]	85.7[31]
				previous calculation	5.039	5.039	17.456[32]	
				experimental	4.99	4.99	17.06[13]	78.0[33]
				experimental	4.988	4.988	17.061[30]	73.5[34]
				experimental	4.991	4.991	17.062[35]	
aragonite	$Pmcn$ (62)	$oP20$	$G0_2$	present work	5.0180	8.0388	5.8155	67.8
				previous calculation	4.8314	7.8359	5.7911[27]	67.7[31]
				previous calculation	5.003	8.047	5.659[30]	66.8[36]
				previous calculation	5.112	8.230	5.915[32]	
				previous calculation	4.9609	7.9936	5.7020[37]	
				experimental	4.9633	7.9703	5.7441[24]	66.8[33]
				experimental	4.961	7.967	5.741[30]	64.8[38]
				experimental	4.962	7.969	5.743[39]	
				experimental	4.9614	7.9671	5.7404[40]	
vaterite	$Pbnm$ (62)	$oP28$	$S1_2$	present work	4.5423	6.6792	8.5127	70.8
				previous calculation	4.531	6.640	8.477[41]	69.1[31]
				previous calculation	4.43	6.62	8.04[27]	
				previous calculation	4.531	6.640	8.477[41]	
				experimental	4.13	7.15	8.48[25]	63.8[42]

Table 2. Surface Energies (J/m^2) of Calcite, Aragonite, and Vaterite Reported in Literature Works and Calculated Values in This Work

surfaces	Leeuw et al.[27]	Sekkal et al.[31]	Massaro et al.[37]	Bano et al.[43]	Rohl et al.[44]	Massaro et al.[45]	Aquilano[46]	Bruno[47]	present work
calcite(10.4)	0.59	0.71		0.7113	0.534	0.536	0.536	0.503	
aragonite(011)CO_3	0.69	0.90	0.801						0.636
aragonite(011)Ca			0.578						0.469
aragonite(011)				0.8406					
vaterite(010)CO_3	0.62	0.75							

energies of $CaCO_3$ polymorphs have been investigated and compared by Leeuw and Parker,[27] Sekkal and Zaoui,[31] Massaro et al.[37] Based on these data (refer to Table 2), the calcite(10.4) and CO_3^{2-} terminated vaterite(010) can be identified as the most stable surfaces for both polymorphs. For aragonite, although the literature works[27,37,43] consent that the (011) plane is the most stable surface, it is still controversial for its termination, namely, CO_3^{2-}[27] and Ca^{2+}[27,37,43] terminations (illustrated in Figure 2) are both reported as the most stable configurations. Therefore, we recalculated the surface energies of both terminations. The surface energy (γ_s) of aragonite(011) is ascertained as

$$\gamma_s = \frac{1}{2A_s}\left(E^{slab}_{aragonite(011)} - n_{CaCO_3}E^{bulk}_{aragonite}\right) \quad (1)$$

where A_s denotes the surface area, n_{CaCO_3} is the number of $CaCO_3$ formula contained in the surface slab, and $E^{slab}_{aragonite(011)}$ and $E^{bulk}_{aragonite}$ are total energies of aragonite(011) surface slab and bulk aragonite per formula, respectively. Our calculated data are also listed in Table 2, and the values are 0.636 and 0.469 J/m^2 for CO_3^{2-} and Ca^{2+} terminations, respectively. This result indicates that Ca^{2+} termination will be more stable for aragonite(011), which is in line with the data of Massaro et al.[37]

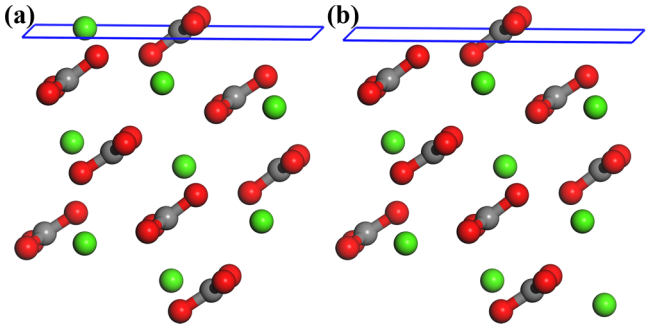

Figure 2. Two different terminations of aragonite(011): (a) terminated with Ca^{2+} and (b) terminated with CO_3^{2-}. Different color spheres denote Ca (green), O (red), C (dark gray), and H (white) atoms.

As aforementioned, the surfaces calcite(10.4), aragonite(011)Ca, and vaterite(010)CO_3 are identified as stable surfaces for the three polymorphs. Consequently, the adsorptions of CH_4 and CO_2 are compared on these three surfaces in the following parts.

The surface slabs are created on the basis of optimized bulk structures. The supercells of calcite(10.4), aragonite(011)Ca, and vaterite(010)CO_3 are modeled as (1 × 2), (2 × 1), and (1 × 2) slabs, respectively. Their surface areas are 8.2 × 10.1, 10.0 × 9.9, and 8.5 × 9.1 Å^2, respectively. To avoid the imaginary interaction between top and bottom sides, a 30 Å vacuum

https://dx.doi.org/10.1021/acsomega.0c00345
ACS Omega 2020, 5, 11369−11377

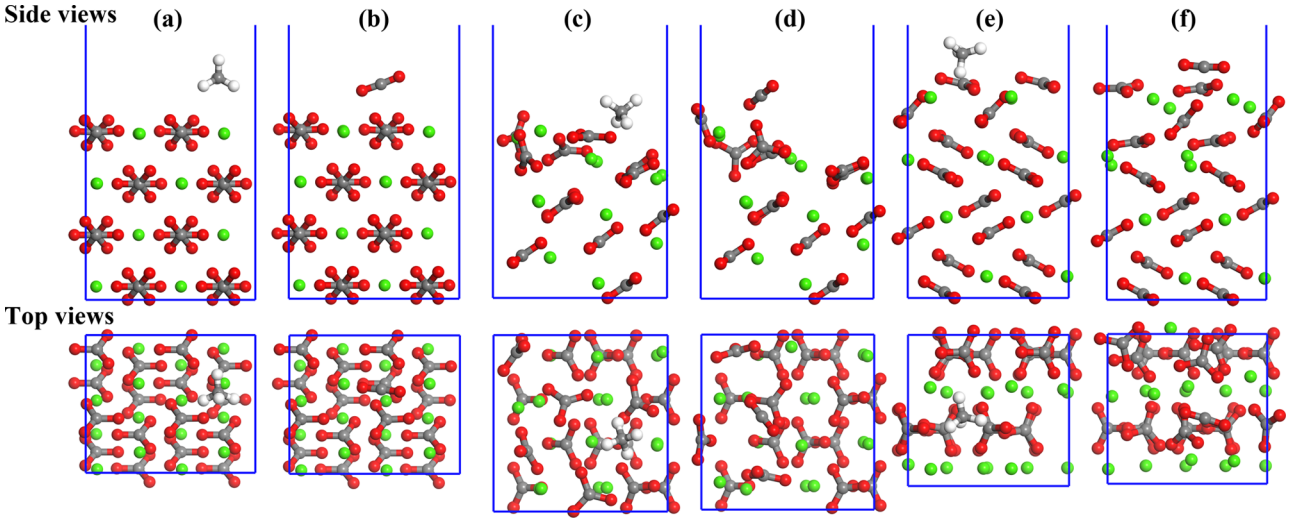

Figure 3. Fully relaxed configurations of CH_4 and CO_2 adsorbed on $CaCO_3$ polymorphs: (a) CH_4 on calcite(10.4), (b) CO_2 on calcite(10.4), (c) CH_4 on aragonite(011)Ca, (d) CO_2 on aragonite(011)Ca, (e) CH_4 on vaterite(010)CO_3, and (f) CO_2 on vaterite(010)CO_3. Different color spheres denote Ca (green), O (red), C (dark gray), and H (white) atoms.

space is inserted in all surface models in depth. The calcite(10.4) slab contains four layers of CO_3^{2-} and Ca^{2+}; the top two layers are free to relax, and the bottom two layers are constrained. For the Ca-terminated aragonite(011), eight layers of Ca^{2+} and eight layers of CO_3^{2-} are included, and the bottom part (four layers of Ca^{2+} and four layers of CO_3^{2-}) is frozen and the rest are free to move. For the CO_3-terminated vaterite(010), four layers of Ca^{2+} and eight layers of CO_3^{2-} are used to mimic the surface, and the bottom two layers of Ca^{2+} and four layers of CO_3^{2-} are fixed to exhibit a bulklike interior.

The interface models are established by putting one molecule on the surfaces. Assuming that each Ca atom on the surface is an adsorption site for a molecule, all of the above configurations correspond to 0.25 ML coverage. First, the interface models are optimized using the MD method by employing COMPASS forcefield. Then, the DFT geometry optimizations are continually conducted to achieve equilibrium states of the adsorption systems.

2.3. Equilibrium Configurations and Adsorption Energies. After the calculations of MD and DFT procedures, the equilibrium configurations of adsorption systems can be achieved (as shown in Figure 3).

For all three $CaCO_3$ polymorphs, surface reconstruction can be observed in the equilibrium models. Especially for aragonite(011)Ca and vaterite(010)CO_3, surface reconstruction is more obvious. This phenomenon is consistent with the previous studies that the absorbed molecules (CO_2[20] and H_2O[48−50]) influence the surface reconstruction of calcite(10.4).

Based on these fully optimized interfacial configurations, the adsorption energies (E_{ad}) can be ascertained as[51]

$$E_{ad} = E_{interface} - E_{surface} - E_{molecule} \quad (2)$$

where $E_{interface}$, $E_{surface}$, and $E_{molecule}$ denote the energies of the interface slab, surface slab, and adsorbed molecule, respectively. The calculated results are listed in Table 3. Our calculated E_{ad} is −51.04 kJ/mol for the system of CO_2 adsorbed on calcite(10.4), which is very close to the previous experimental study (52−67 kJ/mol).[52] So, our calculation results are accurate and reasonable.

Table 3. Calculated Adsorption Energies (E_{ad}) of CH_4 and CO_2 on Calcite(10.4), Aragonite(011)Ca, and Vaterite(010)CO_3 Surfaces

	E_{ad} of molecules (kJ/mol)	
surfaces	CH_4	CO_2
calcite(10.4)	−22.75	−51.04
aragonite(011)Ca	−35.01	−52.94
vaterite(010)CO_3	−27.94	−74.79

If the adsorption energy is negative, the adsorption process will occur spontaneously, which also means that it is an exothermic process. Moreover, the relation between adsorption energy (E_{ad}) and binding energy (E_b) can be expressed as $E_b = -E_{ad}$.[5353] So, if the adsorption energy is more negative, then the adsorption process will have larger potential (or driving force) and will tend to form stronger binding with the adsorbent. By examining our calculated results within this theorem, the following statements can be concluded:

(1) The adsorption energies of CH_4 and CO_2 on calcite(10.4), aragonite(011)Ca, and vaterite(010)CO_3 surfaces are always negative, which suggests that the adsorptions are spontaneous and exothermic processes.
(2) The E_{ad} of CO_2 are more negative than those of CH_4; therefore, compared with CH_4, the interfacial interaction between CO_2 and $CaCO_3$ surfaces should be stronger. This statement is also consistent with the previous studies.[22,23,54]
(3) By comparing E_{ad} values of the same molecule on different surfaces, the adsorption precedence of the three surfaces can be described as follows: (i) for CH_4, the sequence is aragonite(011)Ca > vaterite(010)CO_3 > calcite(10.4); (ii) for CO_2, the sequence is vaterite(010)CO_3 > aragonite(011)Ca > calcite(10.4).

2.4. Mulliken Population and Atomic Configuration Analyses. The Mulliken population analysis is commonly employed in the DFT adsorption investigations.[55−57] Although the absolute values of the atomic charges generated by the population analysis are regarded to have a little physical meaning, these values are strongly influenced by the atomic

https://dx.doi.org/10.1021/acsomega.0c00345
ACS Omega 2020, 5, 11369−11377

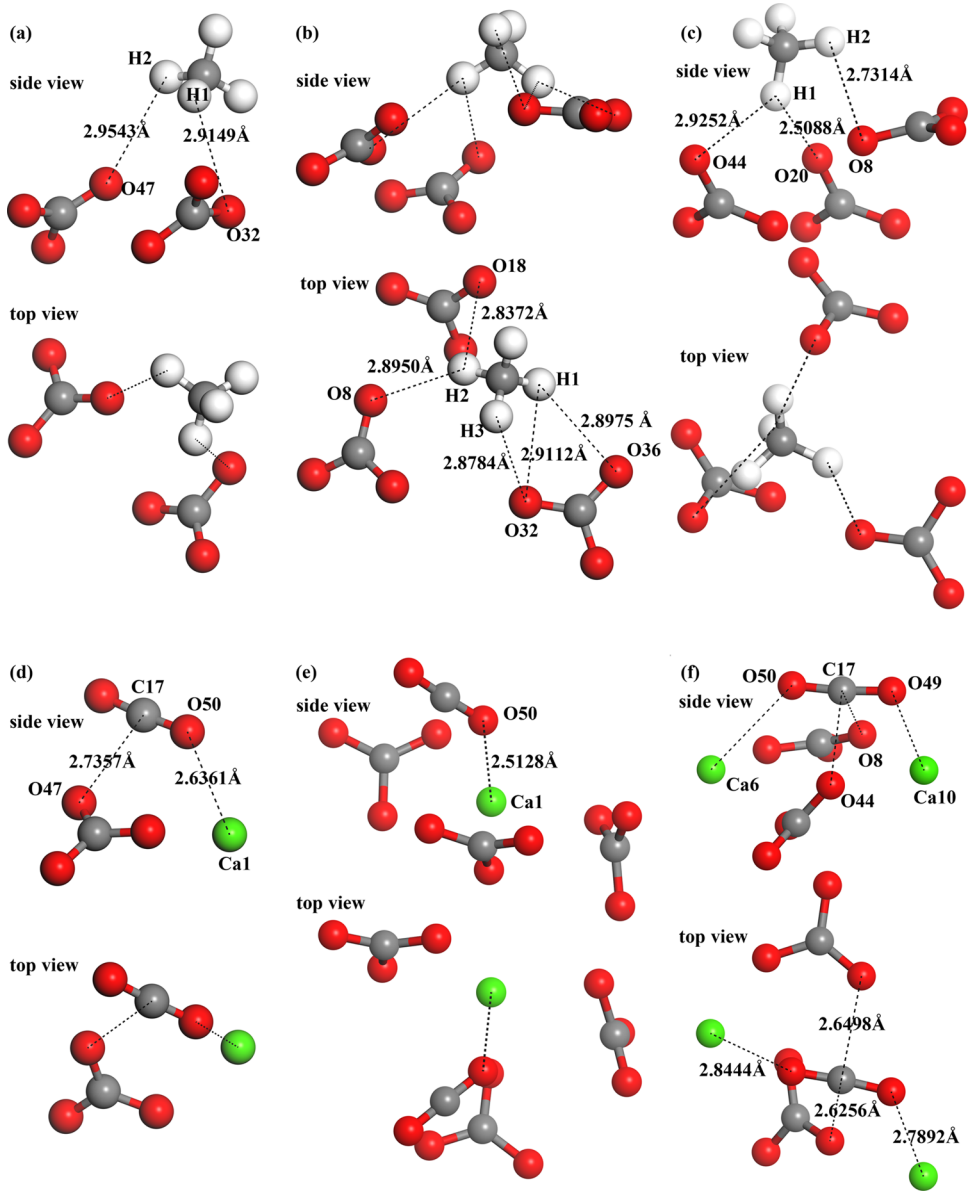

Figure 4. Interfacial atomic configurations of six models: (a) CH_4 on calcite(10.4), (b) CH_4 on aragonite(011)Ca, (c) CH_4 on vaterite(010)CO_3, (d) CO_2 on calcite(10.4), (e) CO_2 on aragonite(011)Ca, and (f) CO_2 on vaterite(010)CO_3. Different color spheres denote Ca (green), O (red), C (dark gray), and H (white) atoms.

basis set with which the DFT calculations were conducted.[58] However, consideration of their relative values can yield useful information.[59−61]

In the present work, Mulliken populations have been calculated for these equilibrium interfacial models. By examining the final atomic configurations together with the Mulliken population analysis, some implications can be obtained, and more importantly, these implications are helpful to shed light on the adsorption mechanism. The interfacial atomic configurations are shown in Figure 4. The results of the Mulliken atomic charge and overlap population are summarized in Tables 4 and 5, respectively. The overlap population may be useful to assess the bond nature; the bond's covalency level increases with an increase in positive values, while negative values suggest an antibonding state.[59,60] To clarify the interfacial interaction nature, the analysis is focused on the adsorbed molecules and some atoms in neighboring surface ions.

The Mulliken charge distribution (Table 4) indicates that the H atoms in CH_4 act as charge donors and O atoms act as charge acceptors. For the atoms in the surface ions, the O atoms in CO_3^{2-} act as charge acceptors and Ca atoms act as charge donors. So, the interfacial interactions between H in CH_4 and O in CO_3^{2-} (likewise between O in CO_2 and surface Ca^{2+}) can be assumed.

The bond population results in Table 5 support the above assumption. Especially for the atom pairs of O in CO_2 and surface Ca, their bond populations are positive values (0.03−0.06), which indicates that weak bonds form between the atoms. As for the atom pairs of H in CH_4 and O in CO_3^{2-}, the bond population values are basically negative around zero, so the interactions between them are mainly electrostatic effects. Therefore, the adsorptions of CH_4 and CO_2 on $CaCO_3$ polymorphs can be featured as physisorption and chemisorptions, respectively. This is also the reason why CO_2

https://dx.doi.org/10.1021/acsomega.0c00345
ACS Omega 2020, 5, 11369−11377

Table 4. Mulliken Charge Distribution in Adsorbed Molecules (CH_4, CO_2) and Some Atoms in Neighboring Surface Ions (Ca^{2+}, CO_3^{2-})[a]

			atomic population				
absorption systems	atoms' origin	atom no.	s	p	d	total	charge (e)
CH_4 on calcite(10.4)	CH_4	C17	1.48	3.61		5.09	−1.09
		H1	0.74	0.00		0.74	0.26
		H2	0.73	0.00		0.73	0.27
		H3	0.71	0.00		0.71	0.29
		H4	0.77	0.00		0.77	0.23
	CO_3^{2-}	O32	1.81	4.93		6.74	−0.74
		O47	1.81	4.88		6.69	−0.69
CH_4 on aragonite(011)Ca	CH_4	C17	1.47	3.61		5.07	−1.07
		H1	0.76	0.00		0.76	0.24
		H2	0.78	0.00		0.78	0.22
		H3	0.71	0.00		0.71	0.29
		H4	0.73	0.00		0.73	0.27
	CO_3^{2-}	O8	1.81	4.89		6.70	−0.70
		O20	1.82	4.85		6.67	−0.67
		O44	1.83	4.88		6.71	−0.71
CH_4 on vaterite(010)CO_3	CH_4	C17	1.46	3.59		5.05	−1.05
		H1	0.80	0.00		0.80	0.20
		H2	0.75	0.00		0.75	0.25
		H3	0.73	0.00		0.73	0.27
		H4	0.73	0.00		0.73	0.27
	CO_3^{2-}	O8	1.81	4.91		6.71	−0.71
		O18	1.81	4.89		6.70	−0.70
		O32	1.81	4.90		6.71	−0.71
		O36	1.81	4.90		6.71	−0.71
CO_2 on calcite(10.4)	CO_2	C17	0.69	2.33		3.02	0.98
		O49	1.83	4.63		6.46	−0.46
		O50	1.82	4.69		6.51	−0.51
	Ca^{2+}	Ca1	2.12	6.00	0.46	8.58	1.42
	CO_3^{2-}	O47	1.81	4.90		6.71	−0.71
CO_2 on aragonite(011)Ca	CO_2	C17	0.68	2.32		3.00	1.00
		O49	1.84	4.59		6.43	−0.43
		O50	1.81	4.71		6.53	−0.53
	Ca^{2+}	Ca2	2.10	6.00	0.48	8.57	1.43
CO_2 on vaterite(010)CO_3	CO_2	C17	0.71	2.33		3.03	0.97
		O49	1.82	4.68		6.50	−0.50
		O50	1.82	4.66		6.48	−0.48
	Ca^{2+}	Ca6	2.10	6.00	0.51	8.61	1.39
		Ca10	2.10	6.00	0.51	8.61	1.39
	CO_3^{2-}	O8	1.81	4.88		6.69	−0.69
		O44	1.81	4.92		6.73	−0.73

[a]The atom no. is labeled in Figure 4.

adsorptions have larger E_{ad} compared with that of CH_4 adsorptions.

Furthermore, for the models of CO_2 on calcite(10.4) and vateriate(010)CO_3, we noticed that the interactions between C in CO_2 and O in CO_3^{2-} also contribute to their interfacial binding effect. However, their overlap bond populations are around zero, and the interactions between these atoms are mainly electrostatic effects.

Summarily, for the interfacial interaction nature of absorbed molecule and $CaCO_3$ surfaces, the following statements can be deduced:

(1) CH_4 adsorptions on the three $CaCO_3$ polymorphs can be characterized as phsisorptions, and the interfacial interactions are mainly contributed by the electrostatic effects between H in CH_4 and O in CO_3^{2-}.

(2) CO_2 may form chemisorption on the three surfaces, and the interfacial binding effect mainly comes from the bonds between O in CO_2 and Ca^{2+} ions. Besides that, the electrostatic interactions between C in CO_2 and O in CO_3^{2-} also make some contributions.

3. CONCLUSIONS

The adsorptions of CH_4 and CO_2 onto calcite(10.4), aragonite(011)Ca, and vaterite(010)CO_3 are investigated and compared by employing MD and DFT calculations.

(1) In the equilibrium atomic configurations, surface reconstruction is observed.

(2) The calculated adsorption energies (E_{ad}) of CH_4 and CO_2 are always negative for the three substrates, which

https://dx.doi.org/10.1021/acsomega.0c00345
ACS Omega 2020, 5, 11369−11377

Table 5. Mulliken Bond Population for the Atom Pairs between Adsorbed Molecules (CH_4, CO_2) and Neighboring Surface Ions (Ca^{2+}, CO_3^{2-})[a]

absorption systems	atom pairs	overlap population	interatomic length (Å)
CH_4 on calcite(10.4)	H1−O32	−0.01	2.9149
	H2−O47	0.00	2.9543
CH_4 on aragonite(011)Ca	H1−O32	−0.01	2.9112
	H1−O36	0.00	2.8975
	H2−O8	0.00	2.8950
	H2−O18	−0.01	2.8372
	H3−O32	−0.01	2.8784
CH_4 on vaterite(010)CO_3	H1−O20	−0.01	2.5088
	H1−O44	−0.01	2.9252
	H2−O8	−0.01	2.7314
CO_2 on calcite(10.4)	O50−Ca1	0.05	2.6361
	C17−O47	0.01	2.7357
CO_2 on aragonite(011)Ca	O50−Ca2	0.06	2.5128
CO_2 on vaterite(010)CO_3	O49−Ca10	0.03	2.7892
	O50−Ca6	0.03	2.8444
	C17−O8	0.01	2.6498
	C17−O44	0.00	2.6256

[a]The atom no. is shown in Figure 4.

indicates that the adsorptions are exothermic processes and spontaneous in thermodynamics.

(3) Comparing with that of CH_4, the E_{ad} of CO_2 is more negative, which suggests that there is a stronger driving force for the adsorption of CO_2, leading to stronger interfacial interactions after adsorption.

(4) The adsorption precedence for the three surfaces can be confirmed as follows: for CH_4, aragonite(011)Ca > vaterite(010)CO_3 > calcite(10.4); while for CO_2, the sequence is vaterite(010)CO_3 > aragonite(011)Ca > calcite(10.4).

(5) Combining with interfacial atomic configuration analysis, the Mulliken charge distribution and population suggest that the adsorption of CH_4 is physisorption and the interfacial interaction mainly comes from the electrostatic effect between H in CH_4 and O in CO_3^{2-}, while the adsorption of CO_2 is chemisorption and the interfacial binding effect is mainly contributed by the bonds between O in CO_2 and Ca^{2+} and the electrostatic interaction between C in CO_2 and O in CO_3^{2-}.

4. COMPUTATION METHODOLOGY

All DFT calculations were performed with the CASTEP package,[62,63] wherein planewave ultrasoft pseudopotentials[64,65] were employed to describe the cores. The electronic exchange correlation effects were treated within generalized gradient approximation (GGA) in the formalism of the Perdew−Burke−Ernzerhof (PBE) functional.[66] The van der Waals dispersion corrections were included using the semiempirical DFT-D approach with the Tkatchenko and Scheffler (TS) scheme,[67] which can generate accurate results for the adsorption of small molecules on solid surfaces.[68] The Brillouin zone is sampled by the Monkhorst−Pack *k*-point grid.[69] Convergence tests have been conducted to determine the cutoff energy and *k*-point grid separation. The details are described in the Supporting Information.

To ensure that the calculation results of different adsorption systems are comparable, the computation parameters employed in the DFT calculations should be the same (or as close to each other as possible). For this reason, the cutoff energy is fixed as 450 eV in all DFT calculations. Similarly, for the different adsorption systems, the *k*-point grid separation (or actual grid spacing) should be as close to each other as possible, so the grid separation is fixed as 0.03 $Å^{-1}$ in all DFT calculations, and the *k*-points are automatically generated as 8 × 8 × 2, 6 × 4 × 6, and 8 × 4 × 4 for bulk unit cells of calcite, aragonite, and vaterite, respectively. Likewise, the *k*-points are automatically set as 4 × 3 × 1, 3 × 3 × 1, and 4 × 4 × 1 for the adsorption systems on the substrates of calcite(10.4), aragonite(011)Ca, and vaterite(010)CO_3 respectively. We also noticed that the cutoff energy of 450 eV and *k*-point grid separation of around 0.03 $Å^{-1}$ have been successfully implemented in the adsorption system containing the calcite(10.4) surface[70] and calcium carbonate hydrates.[71]

■ ASSOCIATED CONTENT

Supporting Information

The Supporting Information is available free of charge at https://pubs.acs.org/doi/10.1021/acsomega.0c00345.

Convergence tests of computation parameters (cutoff energy and *k*-point grid separation) for bulk aragonite, calcite, and vaterite (PDF)

■ AUTHOR INFORMATION

Corresponding Authors

Ming Zhang − *School of Petroleum Engineering, Xi'an Shiyou University, Xi'an 710065, China*; Email: zm9729@xsyu.edu.cn

Jian Li − *School of Materials Science and Engineering, Xi'an Shiyou University, Xi'an 710065, China*; orcid.org/0000-0002-5239-9469; Email: lijian@xsyu.edu.cn

Authors

Junyu Zhao − *School of Materials Science and Engineering, Xi'an Shiyou University, Xi'an 710065, China*

Youming Cui − *School of Materials Science and Engineering, Xi'an Shiyou University, Xi'an 710065, China*

Xian Luo − *School of Materials, Northwestern Polytechnical University, Xi'an 710072, China*

Complete contact information is available at: https://pubs.acs.org/10.1021/acsomega.0c00345

Author Contributions

All authors have discussed the results and commented on the manuscript.

Notes

The authors declare no competing financial interest.

■ ACKNOWLEDGMENTS

The authors acknowledge the financial support for the research from the Natural Science Foundation of Shaanxi Province (Program no. 2019JM-388), the Scientific Research Program of Shaanxi Provincial Education Department (Program no. 15JK1570), the Science and Technology Innovation Fund of Xi'an Shiyou University (Program no. 2015BS12), the Youth Innovation Team of Xi'an Shiyou University (no. 2019QNKYCXTD04), and the Materials Science and Engineering of Provincial Advantage Disciplines of Xi'an Shiyou University (no. YS37020203). The authors also

acknowledge the support from the Center for High Performance Computing of Northwestern Polytechnical University.

REFERENCES

(1) Merlini, M.; Hanfland, M.; Crichton, W. A. CaCO3-III and $CaCO_3$-VI, high-pressure polymorphs of calcite: Possible host structures for carbon in the Earth's mantle. *Earth Planet. Sci. Lett.* **2012**, *333*−*334*, 265−271.
(2) Oganov, A. R.; Ono, S.; Ma, Y.; Glass, C. W.; Garcia, A. Novel high-pressure structures of $MgCO_3$, $CaCO_3$ and CO_2 and their role in Earth's lower mantle. *Earth Planet. Sci. Lett.* **2008**, *273*, 38−47.
(3) Dasgupta, R.; Hirschmann, M. M. The deep carbon cycle and melting in Earth's interior. *Earth Planet. Sci. Lett.* **2010**, *298*, 1−13.
(4) Kim, B.; Park, E.; Choi, K.; Kang, K. Synthesis of $CaCO_3$ using CO_2 at room temperature and ambient pressure. *Mater. Lett.* **2017**, *190*, 45−47.
(5) Kong, H.; Kim, B.; Kang, K. Synthesis of $CaCO_3$−SiO_2 composite using CO_2 for fire retardant. *Mater. Lett.* **2019**, *238*, 278−280.
(6) Zhao, T.; Guo, B.; Zhang, F.; Sha, F.; Li, Q.; Zhang, J. Morphology Control in the Synthesis of $CaCO_3$ Microspheres with a Novel CO_2-Storage Material. *ACS Appl. Mater. Interfaces* **2015**, *7*, 15918−15927.
(7) Yu, C.; Huang, C.; Tan, C. A review of CO_2 capture by absorption and adsorption. *Aerosol Air Qual. Res.* **2012**, *12*, 745−769.
(8) Guo, B.; Zhao, T.; Sha, F.; Zhang, F.; Li, Q.; Zhao, J.; Zhang, J. Synthesis of vaterite $CaCO_3$ micro-spheres by carbide slag and a novel CO_2-storage material. *J. CO_2 Util.* **2017**, *18*, 23−29.
(9) Cui, H.; Zhang, Q.; Hu, Y.; Peng, C.; Fang, X.; Cheng, Z.; Galvita, V. V.; Zhou, Z. Ultrafast and Stable CO_2 Capture Using Alkali Metal Salt-Promoted MgO−$CaCO_3$ Sorbents. *ACS Appl. Mater. Interfaces* **2018**, *10*, 20611−20620.
(10) Nwidee, L. N.; Al-Anssari, S.; Barifcani, A.; Sarmadivaleh, M.; Lebedev, M.; Iglauer, S. Nanoparticles influence on wetting behaviour of fractured limestone formation. *J. Pet. Sci. Eng.* **2017**, *149*, 782−788.
(11) Kabir, S.; Haftbaradaran, R.; Asghari, R.; Sastre, J. Understanding Variable Well Performance in a Chalk Reservoir. *SPE Reservoir Eval. Eng.* **2016**, *19*, 83−94.
(12) Escamilla-Roa, E.; Sainz-Díaz, C. I.; Huertas, F. J.; Hernández-Laguna, A. Adsorption of molecules onto (10-14) dolomite surface: An application of computational studies for microcalorimetry. *J. Phys. Chem. C* **2013**, *117*, 17583−17590.
(13) Ataman, E.; Andersson, M. P.; Ceccato, M.; Bovet, N.; Stipp, S. L. S. Functional group adsorption on calcite: I. oxygen containing and nonpolar organic molecules. *J. Phys. Chem. C* **2016**, *120*, 16586−16596.
(14) Liu, J.; Xi, S.; Chapman, W. G. Competitive Sorption of CO_2 with Gas Mixtures in Nanoporous Shale for Enhanced Gas Recovery from Density Functional Theory. *Langmuir* **2019**, *35*, 8144−8158.
(15) Kabalah-Amitai, L.; Mayzel, B.; Kauffmann, Y.; Fitch, A. N.; Bloch, L.; Gilbert, P. U. P. A.; Pokroy, B. Vaterite Crystals Contain Two Interspersed Crystal Structures. *Science* **2013**, *340*, 454.
(16) Lardge, J. S.; Duffy, D. M.; Gillan, M. J. Investigation of the interaction of water with the calcite (10.4) surface using ab initio simulation. *J. Phys. Chem. C* **2009**, *113*, 7207−7212.
(17) Chun, B. J.; Lee, S. G.; Choi, J. I.; Jang, S. S. Adsorption of carboxylate on calcium carbonate (10-14) surface: Molecular simulation approach. *Colloids Surf., A* **2015**, *474*, 9−17.
(18) Okhrimenko, D. V.; Nissenbaum, J.; Andersson, M. P.; Olsson, M. H. M.; Stipp, S. L. S. Energies of the adsorption of functional groups to calcium carbonate polymorphs: The importance of −OH and −COOH groups. *Langmuir* **2013**, *29*, 11062−11073.
(19) Ataman, E.; Andersson, M. P.; Ceccato, M.; Bovet, N.; Stipp, S. L. S. Functional group adsorption on calcite: II. nitrogen and sulfur containing organic molecules. *J. Phys. Chem. C* **2016**, *120*, 16597−16607.
(20) Tao, L.; Li, Z.; Wang, G.; Cui, B.; Yin, X.; Wang, Q. Evolution of calcite surface reconstruction and interface adsorption of calcite-CO2 with temperature. *Mater. Res. Express* **2019**, *6*, No. 025035.
(21) Sun, H.; Zhao, H.; Qi, N.; Qi, X.; Zhang, K.; Sun, W.; Li, Y. Mechanistic insight into the displacement of CH_4 by CO_2 in calcite slit nanopores: the effect of competitive adsorption. *RSC Adv.* **2016**, *6*, No. 104456.
(22) Wang, S.; Zhou, G.; Ma, Y.; Gao, L.; Song, R.; Jiang, G.; Lu, G. Molecular dynamics investigation on the adsorption behaviors of H_2O, CO_2, CH_4 and N_2 gases on calcite (1 -1 0) surface. *Appl. Surf. Sci.* **2016**, *385*, 616−621.
(23) Eliebid, M.; Mahmoud, M.; Shawabkeh, R.; Elkatatny, S.; Hussein, I. A. Effect of CO_2 adsorption on enhanced natural gas recovery and sequestration in carbonate reservoirs. *J. Nat. Gas Sci. Eng.* **2018**, *55*, 575−584.
(24) Carteret, C.; De La Pierre, M.; Dossot, M.; Pascale, F.; Erba, A.; Dovesi, R. The vibrational spectrum of $CaCO_3$ aragonite: A combined experimental and quantum-mechanical investigation. *J. Chem. Phys.* **2013**, *138*, No. 014201.
(25) Meyer, H. J. Uber Vaterit und seine Struktur. *Angew. Chem.* **1959**, *71*, 678.
(26) Christy, A. G. A Review of the structures of vaterite: The impossible, the possible, and the likely. *Cryst. Growth Des.* **2017**, *17*, 3567−3578.
(27) de Leeuw, N. H.; Parker, S. C. Surface Structure and Morphology of Calcium Carbonate Polymorphs Calcite, Aragonite, and Vaterite: An Atomistic Approach. *J. Phys. Chem. B* **1998**, *102*, 2914−2922.
(28) Elstnerová, P.; Friák, M.; Fabritius, H. O.; Lymperakis, L.; Hickel, T.; Petrov, M.; Nikolov, S.; Raabe, D.; Ziegler, A.; Hild, S.; Neugebauer, J. Ab initio study of thermodynamic, structural, and elastic properties of Mg-substituted crystalline calcite. *Acta Biomater.* **2010**, *6*, 4506−4512.
(29) Ungureanu, C. G.; Cossio, R.; Prencipe, M. An Ab-initio assessment of thermo-elastic properties of $CaCO_3$ polymorphs: Calcite case. *CALPHAD: Comput. Coupling Phase Diagrams Thermochem.* **2012**, *37*, 25−33.
(30) Raiteri, P.; Gale, J. D.; Quigley, D.; Rodger, P. M. Derivation of an Accurate Force-Field for Simulating the Growth of Calcium Carbonate from Aqueous Solution: A New Model for the Calcite−Water Interface. *J. Phys. Chem. C* **2010**, *114*, 5997−6010.
(31) Sekkal, W.; Zaoui, A. Nanoscale analysis of the morphology and surface stability of calcium carbonate polymorphs. *Sci. Rep.* **2013**, *3*, No. 1587.
(32) Akiyama, T.; Nakamura, K.; Ito, T. Atomic and electronic structures of $CaCO_3$ surfaces. *Phys. Rev. B* **2011**, *84*, No. 085428.
(33) Salje, E.; Viswanathan, K. The phase diagram calcite-aragonite as derived from the crystallographic properties. *Contrib. Mineral. Petrol.* **1976**, *55*, 55−67.
(34) Redfern, S. A. T.; Angel, R. J. High-pressure behaviour and equation of state of calcite, $CaCO_3$. *Contrib. Mineral. Petrol.* **1999**, *134*, 102−106.
(35) Maslen, E. N.; Streltsov, V. A.; Streltsova, N. R. X-ray study of the electron density in calcite, $CaCO_3$. *Acta Crystallogr., Sect. B: Struct. Sci.* **1993**, *49*, 636−641.
(36) Ungureanu, C. G.; Prencipe, M.; Cossio, R. Ab initio quantum-mechanical calculation of $CaCO_3$ aragonite at high pressure: thermodynamic properties and comparison with experimental data. *Eur. J. Mineral.* **2010**, *22*, 693−701.
(37) Massaro, F. R.; Bruno, M.; Rubbo, M. Surface structure, morphology and (110) twin of aragonite. *CrystEngComm* **2014**, *16*, 627−635.
(38) Martinez, I.; Zhang, J.; Reeder, R. J. In situ X-ray diffraction of aragonite and dolomite at high pressure and high temperature: Evidence for dolomite breakdown to aragonite and magnesite. *Am. Mineral.* **1996**, *81*, 611−624.
(39) Balmain, J.; Hannoyer, B.; Lopez, E. Fourier transform infrared spectroscopy (FTIR) and X-ray diffraction analyses of mineral and organic matrix during heating of mother of pearl (nacre) from the shell of the mollusc *Pinctada maxima*. *J. Biomed. Mater. Res.* **1999**, *48*, 749−754.

https://dx.doi.org/10.1021/acsomega.0c00345
ACS Omega 2020, 5, 11369−11377

(40) Devilliers, J. P. Crystal structures of aragonite, strontianite, and witherite. *Am. Mineral.* **1971**, *56*, 758−767.
(41) Medeiros, S. K.; Albuquerque, E. L.; Maia, F. F.; Caetano, E. W. S., Jr.; Freire, V. N. First-principles calculations of structural, electronic, and optical absorption properties of $CaCO_3$ Vaterite. *Chem. Phys. Lett.* **2007**, *435*, 59−64.
(42) Maruyama, K.; Kagi, H.; Komatsu, K.; Yoshino, T.; Nakano, S. Pressure-induced phase transitions of vaterite, a metastable phase of $CaCO_3$. *J. Raman Spectrosc.* **2017**, *48*, 1449−1453.
(43) Bano, A. M.; Rodger, P. M.; Quigley, D. New Insight into the Stability of $CaCO_3$ Surfaces and Nanoparticles via Molecular Simulation. *Langmuir* **2014**, *30*, 7513−7521.
(44) Rohl, A. L.; Wright, K.; Gale, J. D. Evidence from surface phonons for the (2 × 1) reconstruction of the (10-14) surface of calcite from computer simulation. *Am. Mineral.* **2003**, *88*, 921−925.
(45) Roberto, M. F.; Marco, B.; Dino, A. Effect of the Surface Relaxation on the Theoretical Equilibrium Shape of Calcite. 1. The [001] Zone. *Cryst. Growth Des.* **2010**, *10*, 4096−4100.
(46) Aquilano, D.; Bruno, M.; Massaro, F. R.; Rubbo, M. Theoretical Equilibrium Shape of Calcite. 2. [-441] Zone and Its Role in Biomineralization. *Cryst. Growth Des.* **2011**, *11*, 3985−3993.
(47) Bruno, M.; Massaro, F. R.; Prencipe, M.; Aquilano, D. Surface reconstructions and relaxation effects in a centre-symmetrical crystal: the {00.1} form of calcite ($CaCO_3$). *CrystEngComm* **2010**, *12*, 3626−3633.
(48) Baltrusaitis, J.; Grassian, V. H. Calcite (10-14) surface in humid environments. *Surf. Sci.* **2009**, *603*, L99−L104.
(49) Villegas-Jiménez, A.; Mucci, A.; Whitehead, M. A. Theoretical Insights into the Hydrated (10.4) Calcite Surface: Structure, Energetics, and Bonding Relationships. *Langmuir* **2009**, *25*, 6813−6824.
(50) Kendall, T. A.; Martin, S. T. Water-Induced Reconstruction that Affects Mobile Ions on the Surface of Calcite. *J. Phys. Chem. A* **2007**, *111*, 505−514.
(51) Zhu, B.; Zhang, L.; Xu, D.; Cheng, B.; Yu, J. Adsorption investigation of CO_2 on g-C_3N_4 surface by DFT calculation. *J. CO_2 Util.* **2017**, *21*, 327−335.
(52) Tabrizy, V. A.; Hamouda, A. A.; Soubeyrand-Lenoir, E.; Denoyel, R. CO2 Adsorption Isotherm on Modified Calcite, Quartz, and Kaolinite Surfaces: Surface Energy Analysis. *Pet. Sci. Technol.* **2013**, *31*, 1532−1543.
(53) Würger, T.; Heckel, W.; Sellschopp, K.; Müller, S.; Stierle, A.; Wang, Y.; Noei, H.; Feldbauer, G. Adsorption of acetone on rutile TiO_2: A DFT and FTIRS study. *J. Phys. Chem. C* **2018**, *122*, 19481−19490.
(54) Duan, S.; Gu, M.; Du, X.; Xian, X. Adsorption Equilibrium of CO_2 and CH_4 and Their Mixture on Sichuan Basin Shale. *Energy Fuels* **2016**, *30*, 2248−2256.
(55) Chandiramouli, R.; Nagarajan, V. Adsorption studies of NH_3 molecules on functionalized germanene nanosheet - A DFT study. *Chem. Phys. Lett.* **2016**, *665*, 22−30.
(56) Chandiramouli, R.; Srivastava, A.; Nagarajan, V. NO adsorption studies on silicene nanosheet: DFT investigation. *Appl. Surf. Sci.* **2015**, *351*, 662−672.
(57) Nagarajan, V.; Chandiramouli, R. NO_2 adsorption behaviour on germanene nanosheet: A first-principles investigation. *Superlattices Microstruct.* **2017**, *101*, 160−171.
(58) Davidson, E. R.; Chakravorty, S. A test of the Hirshfeld definition of atomic charges and moments. *Theor. Chim. Acta* **1992**, *83*, 319−330.
(59) Segall, M. D.; Pickard, C. J.; Shah, R.; Payne, M. C. Population analysis in plane wave electronic structure calculations. *Mol. Phys.* **1996**, *89*, 571−577.
(60) Segall, M. D.; Shah, R.; Pickard, C. J.; Payne, M. C. Population analysis of plane-wave electronic structure calculations of bulk materials. *Phys. Rev. B* **1996**, *54*, 16317−16320.
(61) Winkler, B. O.; Pickard, C. J.; Segall, M. D.; Milman, V. Density-functional study of charge disordering in Cs_2Au(I) Au(III)-Cl_6 under pressure. *Phys. Rev. B* **2001**, *63*, No. 214103.
(62) Segall, M. D.; Lindan, P. J. D.; Probert, M. J.; Pickard, C. J.; Hasnip, P. J.; Clark, S. J.; Payne, M. C. First-principles simulation: ideas, illustrations and the CASTEP code. *J. Phys.: Condens. Matter* **2002**, *14*, 2717.
(63) Clark, S. J.; Segall, M. D.; Pickard, C. J.; Hasnip, P. J.; Probert, M. J.; Refson, K.; Payne, M. C. First principles methods using CASTEP. *Z. Kristallogr.* **2005**, *220*, 567−570.
(64) Vanderbilt, D. Soft self-consistent pseudopotentials in a generalized eigenvalue formalism. *Phys. Rev. B* **1990**, *41*, 7892−7895.
(65) Laasonen, K.; Pasquarello, A.; Car, R.; Lee, C.; Vanderbilt, D. Car-Parrinello molecular dynamics with Vanderbilt ultrasoft pseudopotentials. *Phys. Rev. B* **1993**, *47*, 10142−10153.
(66) Perdew, J. P.; Burke, K.; Ernzerhof, M. Generalized Gradient Approximation Made Simple. *Phys. Rev. Lett.* **1996**, *77*, 3865−3868.
(67) Tkatchenko, A.; Scheffler, M. Accurate Molecular Van Der Waals Interactions from Ground-State Electron Density and Free-Atom Reference Data. *Phys. Rev. Lett.* **2009**, *102*, No. 073005.
(68) Wang, W.; Fan, L.; Wang, G.; Li, Y. CO_2 and SO_2 sorption on the alkali metals doped CaO(100) surface: A DFT-D study. *Appl. Surf. Sci.* **2017**, *425*, 972−977.
(69) Monkhorst, H. J.; Pack, J. D. Special points for Brillouin-zone integrations. *Phys. Rev. B* **1976**, *13*, 5188−5192.
(70) Pinto, H.; Haapasilta, V.; Lokhandwala, M.; Öberg, S.; Foster, A. S. Adsorption and migration of single metal atoms on the calcite (10.4) surface. *J. Phys.: Condens. Matter* **2017**, *29*, No. 135001.
(71) Zhou, Y.; Liu, Q.; Hu, M.; Xu, G.; Xu, R.; Chong, X.; Feng, J. Investigation on the stability, electronic, optical, and mechanical properties of novel calcium carbonate hydrates via first-principles calculations. *Int. J. Quantum Chem.* **2020**, No. e26219.

https://dx.doi.org/10.1021/acsomega.0c00345
ACS Omega 2020, 5, 11369−11377